

High Selectivity Filter Employing Stepped Impedance Resonators, Series Capacitors and Defected Ground Structures for Ultra Wide Band Applications

Chettiparampil J. Bindu^{1, *}, Shanta Mridula¹, and Pezholil Mohanan²

Abstract—The paper presents a compact planar Ultra Wide Band filter employing folded stepped impedance resonators with series capacitors and dumb bell shaped defected ground structures. An interdigital quarter wavelength coupled line is used for achieving the band pass characteristics. The transmission zeros are produced by stepped impedance resonators. The filter has steep roll off rate and good attenuation in its lower and upper stop bands, contributed by the series capacitor and defected ground structures respectively.

1. INTRODUCTION

Ultra Wide Band (UWB) is a promising Wireless Personal Area Networking (WPAN) technology for transmitting data at very high rates using very low power with wide bandwidth. Low power density enables UWB to coexist with Bluetooth, 802.11a/b/g and other current and future wireless systems [1]. Compact and high performance filters are a crucial part of nearly every UWB microwave system, for both confining the spectrum and for improving the front end characteristics of an antenna. It is a challenging task to design a filter which maintains reasonably good and steady performance characteristics over the entire 7.5 GHz wide band extending from 3.1–10.6 GHz. Conventional methods lead to increased order of the filter to attain sharp roll off rate and good stop band attenuation. This results in increased size and complexity of the structure. Different planar filter configurations have been reported for UWB applications, in the last decade. Most common techniques for UWB filter design employ short/open stubs or cascaded high pass and low pass filters [2–5]. Traditional microstrip filter designs in UWB require very small gaps between the coupled segments, causing fabrication difficulty. Filters with improved performance have increased size [6, 7] or are multilayered structures with more number of resonators [8–10]. Issues such as reducing size and simultaneously enhancing the performance have not necessarily been addressed in most of the UWB filter designs.

The lower cut off frequency of an interdigital coupled line filter can be controlled by introducing half wavelength open stubs of varying impedance [11]. A modification with less number of resonators and easily realizable gap between coupled lines is reported in [12]. Further improvement in size is achieved in [13]. This work tries to improve the stop band characteristics and selectivity of a UWB filter by introducing series capacitors and dumb bell shaped Defected Ground Structures (DGS), without increasing the size and order of the filter. The filter employs a flexible design with an interdigital coupled line structure and stepped impedance resonators (SIR) in folded form to make the structure compact. The SIR helps to get adjustable transmission zeros to realize the desired band. The structure exhibits sharp roll off at both lower and upper cut off frequencies and flat group delay in the pass band.

Received 31 January 2014, Accepted 16 April 2014, Scheduled 20 April 2014

* Corresponding author: Chettiparampil Janardhanan Bindu (bindudevan@gmail.com).

¹ Division of Electronics Engineering, School of Engineering, Cochin University of Science and Technology, India. ² Department of Electronics, Cochin University of Science and Technology, India.

2. FILTER STRUCTURE

The proposed filter uses interdigital coupled lines quarter guide wavelength ($\lambda_d/4$) long at 6.85 GHz, the centre frequency of the UWB spectrum extending from 3.1–10.6 GHz. The upper edge of the pass band is determined by the length of the interdigital coupled line. The interdigital structure ensures maximum coupling. The required transmission zeros at the lower edge of the pass band are introduced using stepped impedance resonator (SIR) circuits formed by high impedance folded inductive stub along with a low impedance capacitive stub. The open stubs in folded Stepped Impedance Resonators are made half wavelength long at the centre frequency, to realize parallel LC resonant circuit. In comparison with conventional half wavelength stubs, this reduces the required physical length due to change in effective permittivity and hence guide wavelength, thus making the structure more compact. To make the structure still more compact, the inductive stub is folded. The lower cut off frequency of 3.1 GHz is decided by the L and C values which in turn depend on the dimensions of these stubs. The coupled line is made quarter wavelength long at the centre frequency, which determines the upper cut off frequency. The final dimensions are selected after exhaustive experimental and simulation iteration. Methods to improve the filter performance without compromising the size and complexity are analyzed. Figs. 1(a)–(c) show the top and bottom view of the proposed filter structure. Series capacitors are high pass elements. They attenuate lower frequencies. Thus the lower stop band attenuation is improved by introducing an interdigital series capacitor in the transmission line. Considering a line inductance of 1.92 nH plus contribution by the mutual inductance between coupled lines, the required capacitance for

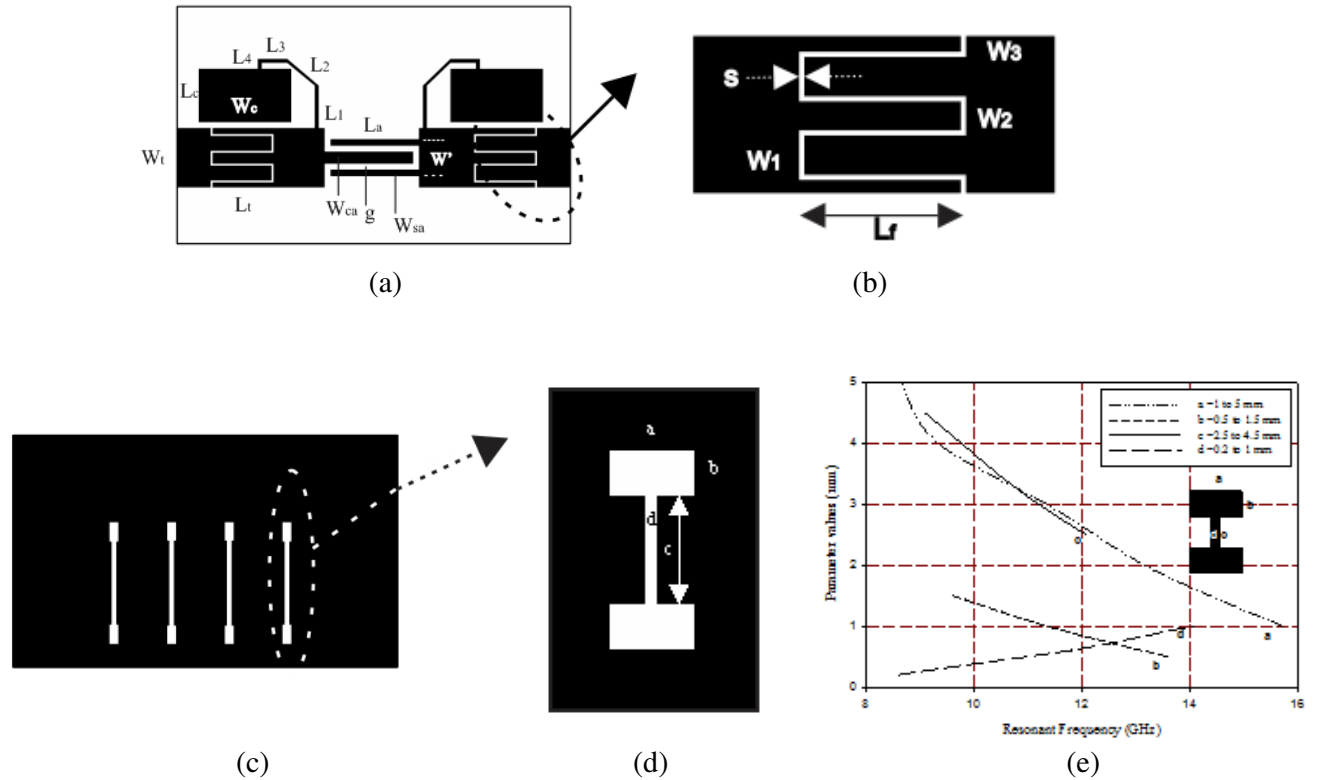


Figure 1. Structural Layout (all dimensions in mm). (a) Top view of the structure — ($L_t = 7.5$, $W_t = 3$, $W_{ca} = 0.61$, $W_{sa} = 0.32$, $W_c = 4.7$, $L_a = 4.5$, $L_1 = 2.15$, $L_2 = 1.95$, $L_3 = 1.5$, $L_4 = 0.7$, $L_c = 2.6$, $W^l = 1.85$, $g = 0.3$; $L_{stub} = L_1 + L_2 + L_3 + L_4$). (b) Enlarged view of interdigital capacitor — ($L_f = 3.2$, $W_1 = 0.8$, $W_2 = 0.6$, $W_3 = 0.2$, $S = 0.1$). (c) Bottom view — ground plane with DGS. (d) Enlarged view of dumb-bell DGS ($a = 0.5$, $b = 1$, $c = 4.3$, $d = 0.24$). (e) Variation of resonant frequency with DGS dimensions.

attenuating frequencies below 3.1 GHz is 0.51 pF. The series capacitance of the interdigital capacitor [15],

$$C = \frac{\epsilon_{re} 10^{-3} K(k)}{18\pi K'(k)} (N - 1) L_f \text{ (pF)} \quad (1)$$

where L_f is the length of the finger in microns, N the number of fingers, and ϵ_{re} the effective dielectric constant of the microstrip line of width equal to the finger width. The ratio

$$\frac{K(k)}{K'(k)} = \frac{\pi}{\ln \left[2 \frac{1 + \sqrt{k'}}{1 - \sqrt{k'}} \right]} \quad k = \tan^2 \left(\frac{a\pi}{4b} \right); \quad a = \frac{W_f}{2}; \quad b = \frac{W_f + S}{2}; \quad k' = \sqrt{1 - k^2}; \quad (2)$$

The design started with symmetric interdigital capacitor, with equal finger width of 0.4 mm and gap width of 0.2 mm. The dimensions are so chosen as to accommodate it in the 3 mm width of the transmission line of the filter. The Eqs. (1)–(3) are used for getting the initial approximate dimensions of the structure. However, fine tuning of the band required changes in the dimensions of the capacitor, resulting in an asymmetric structure. The actual dimensions are shown in the enlarged view in Fig. 1(b), resulting in a capacitance value of 0.66 pF [15, 16]. The introduction of series capacitor seriously affects the insertion loss in the pass band due to its parasitic resistance, whose value is given by the expression

$$R = \frac{4}{3} \frac{L_f}{W_f N} R_s \text{ ohms} \quad (3)$$

where R_s is the sheet resistivity of copper. Exhaustive simulation studies show that the alignment of the series interdigital capacitors only slightly affects the pass band frequency response, but alters the stop band attenuation considerably. The position is so chosen as to optimize the stop band attenuation. In order to compensate for the insertion loss and to get better rejection in the upper stop band, the use of Defected Ground Structures (DGS) is exploited. Dumb bell shaped DGS is employed in this work. The function of DGS is multifold. It is used mainly for improving the upper stop band attenuation by virtue of its property as a parallel LC resonator. The resonant frequency of these circuits are adjusted (by adjusting dimensions a , b , c , and d) to be slightly above (11.5 GHz) the upper cut off frequency to suppress the higher frequencies. The DGS also increases the overall inductance and capacitance of the structure. A larger inductance improves insertion loss, but tends to reduce the upper cut off frequency. The dimensions of various parts of the DGS are shown in the enlarged view of Fig. 1(d). The dimensions ‘ a ’, ‘ b ’ of the dumb bell affect the route length of current and hence change the effective inductance while the dimensions ‘ c ’ and ‘ d ’ affect the accumulation of charge and thus vary the capacitance. They act as series connected parallel LC resonant circuit whose resonant frequency can be adjusted by varying the dimensions. The dependence of resonant frequency of the DGS on dimensional variations of ‘ a ’, ‘ b ’, ‘ c ’ and ‘ d ’ are shown in Fig. 1(e). The dimensions and spacing of the Dumb bell are properly chosen to achieve the required upper stop band characteristics. The spacing between the dumb bells is chosen to be equal to quarter wavelength at the centre frequency.

The structure is simulated using FEM based simulator HFSS from Ansoft Corporation. The overall dimension of the structure including substrate is 20 mm × 12 mm. The simulated transmission and reflection characteristics in Fig. 2 reveal that the insertion loss for the filter is well within 1 dB except for 1.2 dB at 3.68 GHz. The roll off rate is steep and as high as –490 dB/GHz at lower edge and –34 dB/GHz at the upper edge. The out of band rejection obtained is below –18 dB at lower and below –23 dB at upper sides. The insertion loss is minimized by optimizing the gap (g) between the coupled lines.

The surface current and electric field distributions of the top and bottom surface of the structure at various frequencies of interest are shown in Fig. 3 and Fig. 4 respectively. At 3.04 GHz current crowding occurs in SIR thus identifying it as the contributing element for the lower side transmission zero (Fig. 3(a)). The electric field at 3.04 GHz shows the influence of the series capacitor (Fig. 3(b)). The surface current and electric field at the centre frequency 6.85 GHz in Figs. (c)–(d) show that the entire signal is coupled to the output port at 6.85 GHz. Upper side transmission zeros at 11.9 GHz and 13.6 GHz are due to the DGS dimensions as can be observed from the current distributions in bottom ground plane. There is current crowding in the dumb bell heads Figs. 4(a)–(c) showing their inductive behavior. The capacitive nature of the middle portion is clear from the electric field distribution at these frequencies Figs. 4(b)–(d).

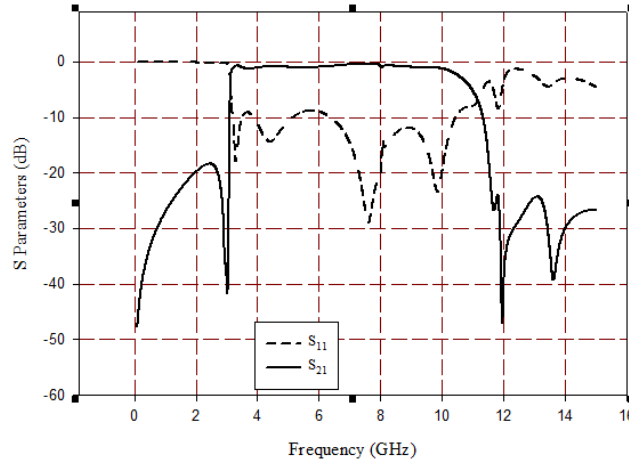


Figure 2. Simulated S parameters.

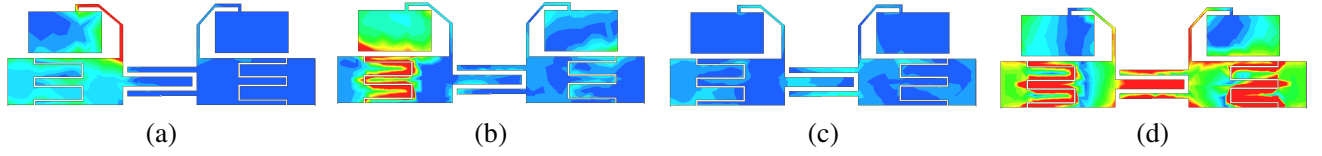


Figure 3. Field distributions on top surface of the structure at various frequencies of interest. (a) Surface current at 3.04 GHz. (b) Electric field at 3.04 GHz. (c) Surface current at 6.85 GHz. (d) Electric field at 6.85 GHz.

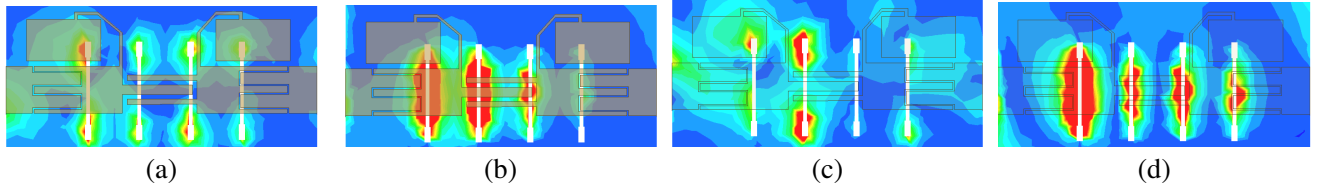


Figure 4. Field distributions on bottom surface at various frequencies of interest. (a) Surface current at 11.9 GHz. (b) Electric field at 11.9 GHz. (c) Surface current at 13.6 GHz. (d) Electric field at 13.6 GHz.

3. DEDUCTION OF LC EQUIVALENT CIRCUIT

Figure 5 shows the LC equivalent circuit of the filter. The values L_1 , C_1 and L_3 , C_3 represent the parallel LC resonators introduced by the folded SIR. C_{int} , L_p and C_p are the capacitance and the parasitic inductance and capacitance of the interdigital coupled line. C_s represents the series capacitance introduced due to the series interdigital capacitor and L_{sp} its parasitic inductance. Its parasitic capacitance is shown included in C_{shunt} , the distributed capacitance of the structure. C_{dgs} and L_{dgs} represent the capacitance and inductance of the defected ground structures. For stepped impedance resonator, a high impedance (Z_{0l}) of 150 and low impedance (Z_{0c}) of 40 are chosen. Two quarter wavelength lines connected end to end form the half wavelength line. Width required for a characteristic impedance of 150 is calculated as 0.2 mm using the relation [14],

$$\frac{W}{h} = \frac{8e^A}{e^{2A} - 2}; \quad \text{where } A = \frac{Z_0}{60} \sqrt{\frac{\epsilon_r + 1}{2}} + \frac{\epsilon_r - 1}{\epsilon_r + 1} \left(0.23 + \frac{0.11}{\epsilon_r} \right) \quad (4)$$

For this width of the microstrip line, the effective permittivity and corresponding guide wavelength (λ_{gl}) are calculated at the centre frequency. The length of the inductive stub is initially chosen as ($\lambda_{gl}/4$).

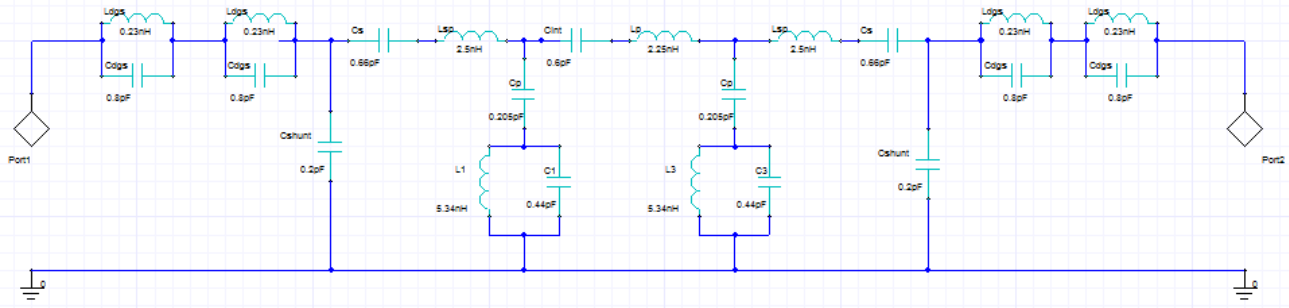


Figure 5. LC equivalent circuit of the filter.

Thus a value of 6.3 mm is chosen and realized in folded form; ($l_l = 6.3 \text{ mm} = (L_1 + L_2 + L_3 + L_4)$). Substituting this in the expression $l_l = f_c \lambda_{gl} L / Z_{0l}$ gives an inductance value of 5.34 nH. Similarly, the width required for the characteristic impedance of 40 is calculated as 4.35 mm using the relation,

$$\frac{W}{h} = \frac{2}{\pi} (B - 1 - \ln(2B - 1)) + \frac{\epsilon_r - 1}{2\epsilon_r} \left(\ln(B - 1) + 0.39 - \frac{0.61}{\epsilon_r} \right); \quad \text{where } B = \frac{377\pi}{2Z_0(\sqrt{\epsilon_r})} \quad (5)$$

The guide wavelength corresponding to this width is $(\lambda_{gc}) = 22.8 \text{ mm}$ at centre frequency 6.85 GHz. The length of the capacitive stub is initially chosen as $(\lambda_{gc}/4)$. Fine tuning of the width and length of this stub leads to a width of 4.7 mm and a length of 2.6 mm for realizing the lower cut off frequency. The value of capacitance for this dimension is computed using the relation, $l_c = f_c \lambda_{gc} Z_{0c} C$ which gives a capacitance value $C = 0.44 \text{ pF}$. The computed values of L and C give rise to a resonant frequency of 3.05 GHz. Series capacitance C_{int} of the interdigital coupled line which has been presented in Fig. 1(a) is evaluated using Eq. (1) [15, 16]. The L_p and C_p in the equivalent circuit model represent conventional series inductance and shunt capacitance in microstrip transmission line and are considered as parasitic elements in interdigital structure. Values of these elements can be obtained from transmission line theory from the length of the structure [15]

$$L_p = \frac{Z_0 \sqrt{\epsilon_{re}}}{c} L_a; \quad C_p = \frac{1}{2} \frac{\sqrt{\epsilon_{re}}}{Z_0 c} L_a \quad (6)$$

where ϵ_{re} is effective relative permittivity of the microstrip transmission line whose strip width is W' , Z_0 the characteristic impedance of a microstrip transmission line with strip width of W' (marked in Fig. 1(a)), and c the velocity of light in free space. The computed values are 2.25 nH (including the mutual inductance between the coupled lines) and 0.205 pF respectively. The defected ground structures etched in the ground plane acts as parallel LC resonant circuit whose resonant frequency is selected as 11.5 GHz, slightly above the cut off frequency. The L and C values are computed based on the desired frequency values using the Eqs. (8)–(9) [17]. A distributed shunt capacitance of 0.2 pF is assumed in the above circuit.

$$C_{dgs} = \frac{\omega_c}{2Z_0(\omega_0^2 - \omega_c^2)}; \quad L_{dgs} = \frac{1}{\omega_0^2 C_{dgs}} \quad (7)$$

4. CIRCUIT ANALYSIS

Optimetric analysis is carried out for varying lengths of inductive stub and coupled arm. As the length of the inductive stub is varied from 5.3 mm to 6.8 mm, the structure shows a shift in lower cut off frequency from 3.4 to 3.08 GHz, as illustrated in Fig. 6(a). The dependence of upper cut off frequency on coupled arm length is illustrated in Fig. 6(b). It is observed that as arm length increases, upper cut off frequency shifts left. Multi variable regression analysis is carried out on simulation results. Design equations which give the dimensions of the controlling elements for the desired lower and upper cut off frequencies are developed. The equations are validated on various substrates having different values of

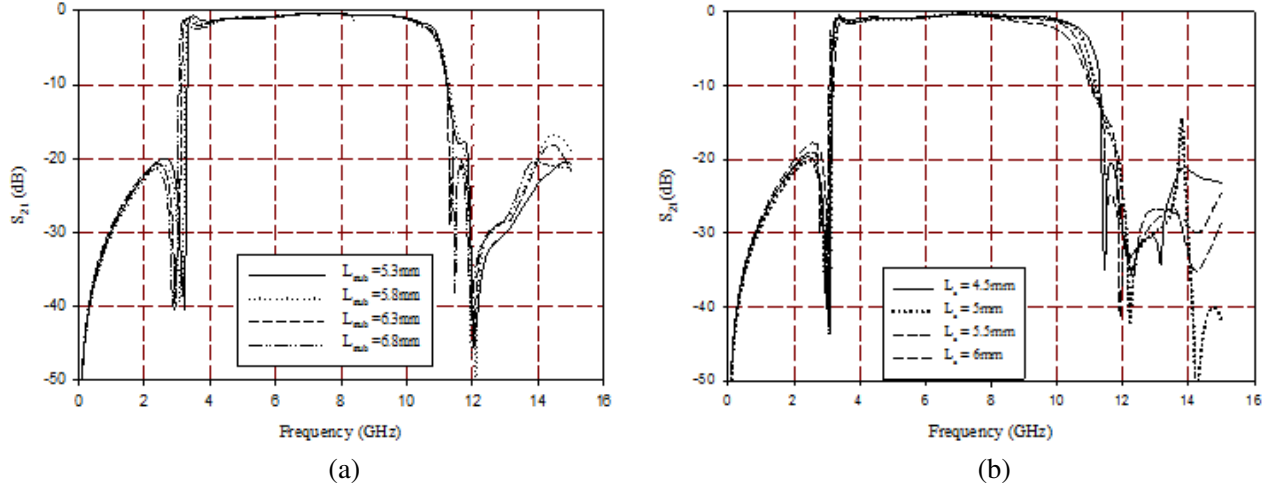


Figure 6. Parametric analysis. (a) Dependence of upper cut off frequency on coupled arm length L_a . (b) Variation of lower cut off frequency with inductive stub length L_{stub} .

permittivity and slab thickness. The length of the folded inductive stub of the SIR for any desired lower cut off frequency can be determined by using the relation,

$$L_{stub} = 33.73 - 4.71f_1 - 1.62\epsilon_r - 3.51h \quad (8)$$

Here L_{stub} is the length of the folded inductive stub in mm, ϵ_r the relative permittivity of the substrate material, h the height of the dielectric slab in mm, and f_1 the lower cut off frequency in GHz. The expression for the coupled arm length L_a required for any upper cut off frequency f_2 is given by

$$L_a = 22.59 - f_2 - 1.1\epsilon_r - 1.35h \quad (9)$$

Table 1 illustrates the designed values of L_{stub} and L_a as per Eq. (8) and Eq. (9) and the bandwidth obtained on different substrates. The equations are valid for the specified dimensions of DGS. The dimensions of interdigital capacitor are also kept unaltered except for substrates which required considerable change in the width of transmission line for proper impedance matching. For these cases, 10% change is required in the dimensions of the finger width. The valid ranges of ϵ_r and h for the equations are limited, as the structure involves series capacitor and DGS. The range can be given as $3.7 \leq \epsilon_r \leq 5.7$; $1.5 \leq h \leq 1.6$.

Table 1. Computed values of L_{stub} and L_a for the UWB operating band on various substrates.

ϵ_r/h	L_{stub}	L_a	Bands Obtained	% Error
3.7/1.6	7.51	5.7	3.04–10.5	1.9/0.9
4.2/1.6	6.70	5.3	3.07–10.5	0.9/0.9
5.2/1.5	5.44	4.2	3.12–10.6	0.6/0
5.7/1.5	4.63	3.6	3.1–10.5	0/0.9

5. FABRICATION AND RESULTS

The filter structure is fabricated on a substrate with relative permittivity of 4.4, dielectric loss tangent of 0.02 and thickness of 1.6 mm. Fig. 7 shows the photograph of the fabricated filter structure along with the SMA connectors. The structure is compact as can be seen in figure. The filter characteristics are measured with Agilent 8362B PNA Network Analyzer. The measured results in Figs. 8(a)–(c) show

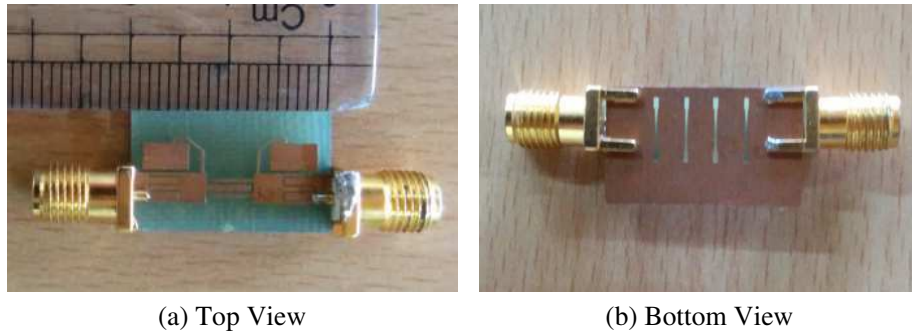


Figure 7. Photograph of the fabricated prototype filter.

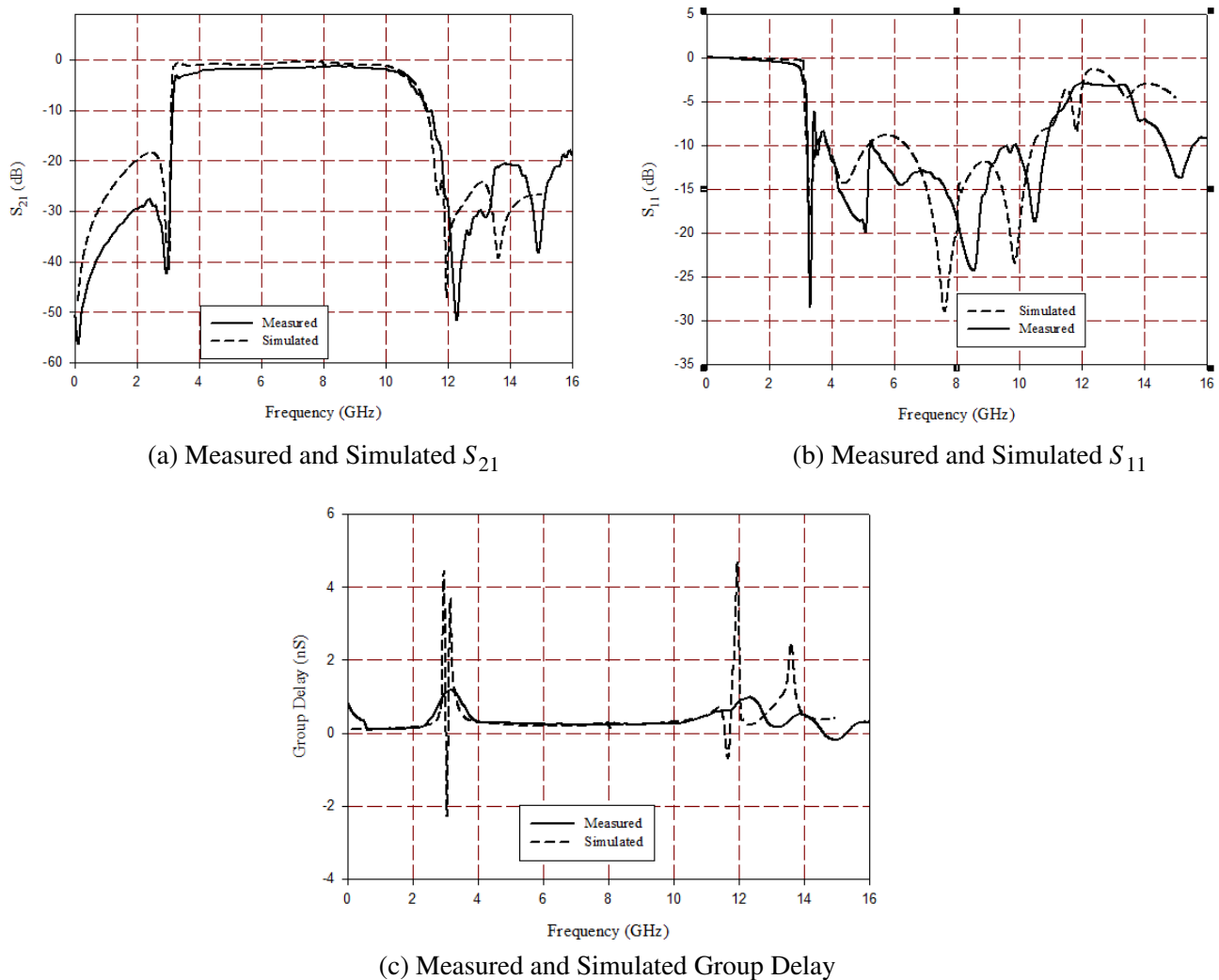


Figure 8. Measured parameters.

good agreement with the simulated results. The small discrepancies in the result can be attributed to the inaccuracies in the fabrication process and/or numerical errors in simulation. The average insertion loss for the fabricated filter in the pass band is -2.5 dB including the connector loss. This can be brought down by using a low loss substrate material. The measured attenuation is better than -28 dB

in the lower stop band and -20 dB in upper stop band. The roll-off rate is sharp with 147 dB/GHz at lower and 30 dB/GHz at upper band edge and the fractional bandwidth attained is approximately 109% . The measured and simulated reflection characteristics are shown in Fig. 8(b). The measured and simulated group delay in Fig. 8(c) show good agreement. Being energy storage elements, the resonators store the energy, rather than passing it out, hence the delay is more at the band edges. The abrupt change in group delay at the cut off frequencies is by the influence of the resonators. The group delay is almost flat in the pass band and has a value less than 0.2 nS. This reveals the linear phase nature of the filter making it suitable for all communication applications.

Table 2 gives a comparison of the performance of the proposed filter with other reported UWB filters [4–7]. As can be observed from the table, the proposed filter is compact and superior in performance with respect to roll off rate and group delay. The actual size neglecting substrate dimension is $20 \text{ mm} \times 6.6 \text{ mm}$.

Table 2. Comparison of parameters of similar works.

Parameters	References				Proposed Filter
	[4]	[5]	[6]	[7]	
Pass band (GHz)	3.6–9.45	3.5–14.5	3.1–10.6	3.3–9.9	3.17–10.6
Insertion Loss (dB)	1–2	0.88–2.4	≤ 1	0.9	2.5
Rolloff Rate-Lower, Upper (dB/GHz)	26, 16	28, 26	28, 22	44, 34	147, 30
Stop band Attenuation-Lower, Upper (dB)	20	Not specified	26, 16	$-60, 36.1$	28, 20
Group Delay (nS)	0.28	0.2	Not specified	0.3	0.2
Size (mm^2)	16.4×6.6	44.8×10.5	34.2×29	25.48×6.42	20×6.6
Substrate [ϵ_r/h]	2.94/0.76	3.38/0.508	2.2/0.508	LCP	4.4/1.6

6. CONCLUSION

The filter designed is simple and can be finely tuned by varying the dimensions of open stubs and coupled lines. The roll off achieved is steep, and the attenuation in the stop bands is reasonable. The proposed filter can be easily integrated to any PCB as that of UWB transceivers, several mass-produced consumer items, spectrum/frequency analyzers, converters used with satellite television dishes, etc.

ACKNOWLEDGMENT

The authors owe a great deal to the experimental facilities extended by Centre for Research in Electromagnetics and Antennas (CREMA), Department of Electronics, CUSAT.

REFERENCES

1. FCC, “Federal communications commission revision of part 15 of the commission’s rules regarding ultra-wideband transmission systems,” *First Report and Order FCC’02*, V48, 2002.
2. Hao, Z. C. and J.-S. Hong, “Ultrawideband filter technologies,” *IEEE Microwave Magazine*, Vol. 11, 56–68, 2011.
3. Weng, L. H., Y. C. Guo, X. W. Shi, and X. Q. Chen, “An overview on defected ground structure,” *Progress In Electromagnetics Research B*, Vol. 7, 173–189, 2008.
4. Song, K. and Q. Xue, “Inductance-loaded Y-shaped resonators and their applications to filters,” *IEEE Trans. Microwave. Theory Tech.*, Vol. 58, No. 4, 978–984, 2010.

5. Wong, W.-T., Y.-S. Lin, C.-H. Wang, and C. H. Chen, "Highly selective microstrip bandpass filters for ultra-wideband (UWB) applications," *Proc. Asia-Pacific Microwave Conference*, Vol. 5, 2850–2853, Dec. 2005.
6. Zong, W., X. Zhu, et al., "Design and implement of compact UWB bandpass filter with a frequency notch by consisting of coupled microstrip line structure, DGS and EOS," *Proc. International Conference on Advanced Technologies for Communications*, 179–182, Oct. 2009.
7. Hao, Z.-C. and J.-S. Hong, "Highly ultra wideband bandpass filters with quasi-elliptic function response," *Microwaves, Antennas & Propagation*, Vol. 5, 1103–1108, 2011.
8. Razalli, M. S., A. Ismail, and M. A. Mahdi, "Novel compact microstrip ultra-wideband filter utilizing short-circuited stubs with less vias," *Progress In Electromagnetics Research*, Vol. 88, No. 4, 91–104, 2008.
9. Chen, L.-N., Y.-C. Jiao, H.-H. Xie, and F.-S. Zhang, "A novel G-shaped slot ultra-wideband bandpass filter with narrow notched band," *Progress In Electromagnetics Research Letters*, Vol. 20, 77–86, 2011.
10. Hsiao, P.-Y. and R.-M. Weng, "Compact tri-layer ultra-wideband band-pass filter with dual notch bands," *Progress In Electromagnetics Research*, Vol. 106, 49–60, 2010.
11. Singh, P. K., S. Basu, and Y.-H. Wang, "Planar ultra-wideband bandpass filter using edge coupled microstrip lines and stepped impedance open stub," *IEEE Microwave and Wireless Components Letters*, Vol. 17, No. 9, 649–651, 2007.
12. Bindu, C. J., S. Mridula, and P. Mohanan, "Compact planar filter for ultra wide band applications," *Proc. Int. Colloquiums on Computer Electronics Electrical Mechanical and Civil*, 114–117, Kochi, India, Sep. 2011.
13. Bindu, C. J. and S. Mridula, "Folded SIR filter with CSRRs for ultra wide band applications," *Proc. International Symposium on Electronic System Design*, 182–185, Singapore, Dec. 2013.
14. Pozar, D. M., *Microwave Engineering*, 2nd Edition, Ch. 8, Wiley, New York, 1998.
15. Bahl, I. J., *Lumped Elements for RF and Microwave Circuits*, Artech House, Inc, Norwood, 2003.
16. Ali, M., A. Kachouri, and M. Samet, "Novel method for planar microstrip antenna matching impedance," *Journal of Telecommunications*, Vol. 2, 131–138, 2010.
17. Guo, Y. and Q. Wang, "An improved parameters extraction method for dumb bell shaped defected ground structure," *Scientific Research Engineering Online Journal*, Vol. 2, 197–200, 2010.